Structure and one-dimensional metallicity of rare-earth silicide nanowires on Si(001)

Kris Holtgrewe,[1,2,*] Stephan Appelfeller,[3] Martin Franz,[3] Mario Dähne,[3] and Simone Sanna[1,2]

[1]*Institut für Theoretische Physik, Justus-Liebig-Universität Gießen, D-35392 Gießen, Germany*
[2]*Center for Materials Research (LaMa), Justus Liebig Universität Gießen, D-35392 Gießen, Germany*
[3]*Institut für Festkörperphysik, Technische Universität Berlin, D-10623 Berlin, Germany*

Rare-earth deposition on Si(001) substrates and thermal treatment lead to the formation of metastable silicide nanowires with extremely high aspect ratios and quasi-one-dimensional metallicity. In this work, the prototypical erbium silicide nanowires are investigated theoretically by *ab initio* thermodynamics, considering a multitude of possible nanowire structures. The calculations indicate that the nanowires consist of hexagonal $ErSi_2$ with two possible orientations with respect to the substrate, that they are partially buried into the substrate, and that they are electronically decoupled from the substrate. However, wires of finite width are predicted to be less favorable than planar silicide structures, demonstrating that the wires are metastable and suggesting that their formation is more governed by kinetic effects than by thermodynamics.

I. INTRODUCTION

Rare-earth (RE) silicide nanowires formed by self-assembly on Si(001) surfaces represent a fascinating system of low-dimensional nanoscale objects with extremely high aspect ratios, which have been studied intensively within the last years [1–20]. They are characterized by a one-dimensional metallicity [6–9], and due to the vanishing electronical coupling with the silicon substrate they may be considered suitable conductors for nanoelectronics applications [10]. Furthermore, they can be isolated from the environment by capping with amorphous silicon without affecting their structural properties, in this way preventing mechanical or chemical disturbances [11,12].

As an example, scanning tunneling microscopy (STM) and angle-resolved photoelectron spectroscopy (ARPES) results for terbium silicide nanowires are shown in Fig. 1. They are characterized by widths of a few nanometers and lengths that may exceed hundreds of nanometers, and they usually form parallel bundles [Fig. 1(a)]. A closer view of the single wires is shown in Fig. 1(b). Moreover, a strong electronic dispersion is observed parallel to the nanowires with bands crossing the Fermi level [Fig. 1(c)]. Very similar results are reported for nanowires formed by other trivalent rare earths [6–9], which is related to their chemical similarity.

The self-assembled growth of the nanowires is controlled by macroscopic parameters such as the amount of deposited RE and the thermal conditions, resulting in a metastable structure, which transforms to larger silicide islands at higher temperatures [9,13,14]. Until now, different structural models and growth mechanisms of the nanowires have been discussed [8,15]. As the substrate acts as an infinite reservoir of silicon atoms, the nanowires are assumed to consist of the silicon richest silicide, being hexagonal and tetragonal $RESi_2$, as

in the case of the silicide structures formed on the Si(111) surface [21]. Indeed, transmission electron microscopy (TEM) data are compatible with the hexagonal [11] or the tetragonal [4] $RESi_2$ structure. However, a distinction between hexagonal and tetragonal nanowires is not meaningful for the usually observed nanowire heights of two atomic layers, because of their identical building blocks. Moreover, it is assumed that the silicon surplus results in a silicon termination of the nanowire surfaces, so that the often observed (2×1) periodicity [Fig. 1(b)] is assigned to the formation of silicon dimers [8].

In most previous studies, nanowire formation was related to anisotropic strain, which is only pronounced for the hexagonal silicide. Since its lattice constant a fits well to the one of the Si(001) surface, while the lattice constant c has a large mismatch of about 7%, it was assumed that the nanowires consist of the hexagonal silicide with its c axis perpendicular to the nanowires [1–3,13,16,17], which, however, was questioned in a recent TEM study [11].

Although many experimental studies have been dedicated to the RE silicide nanowires, a comprehensive and detailed theoretical analysis featuring a comparison of possible nanowire structures and their electronic properties is still missing. Previous theory work has only addressed one atomic layer high nanowires [14,15,18,19] or free-standing nanowires [20], whereby most experimental data suggest a nanowire height of two atomic layers [11,16,17].

In this work, we present density functional theory (DFT) calculations to provide an atomistic description of the RE silicide nanowires and their relative stability. The latter is predicted for systematically varied structure models by *ab initio* thermodynamics. We then compare the simulated STM images and calculated band structures with experimental STM and ARPES data, respectively. Our calculations reveal that the nanowires are thermodynamically metastable, since they tend to form an extended two-dimensional silicide layer and to grow further in height. Thus, the nanowire formation cannot be explained by thermodynamics and is instead attributed to

---

*Corresponding author:
kris.holtgrewe@theo.physik.uni-giessen.de
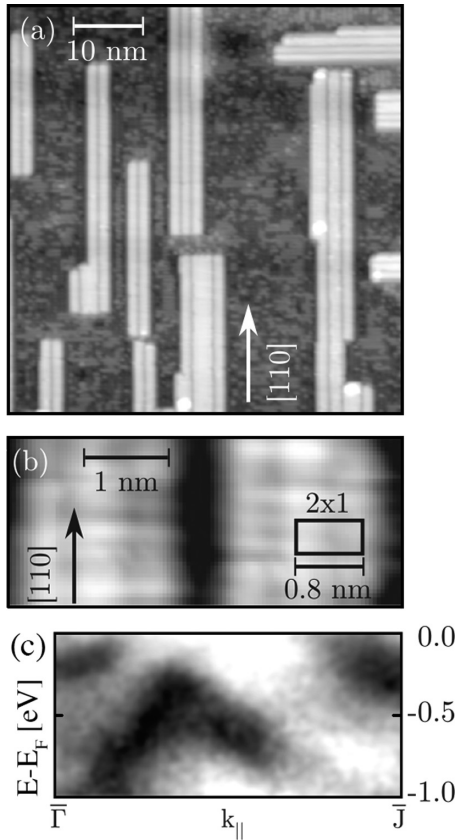
FIG. 1. (a) STM image of Tb silicide nanowires on Si(001) ($V_{\text{sample}} = -2.5$ V, $I = 100$ pA), (b) detailed STM image of one nanowire bundle ($V_{\text{sample}} = -1.5$ V, $I = 100$ pA), (c) ARPES measurement along the nanowires with the most pronounced dispersive bands around $\bar{\Gamma}$ ($k_{\parallel} = 0$) and $\bar{J}$ (edge of nanowire Brillouin zone).

growth kinetics. Among the nanowires of finite width, we find that they grow partially buried into the silicon substrate and have a height depending on the RE availability. The calculated models lead to an atomic and electronic structure compatible with STM and ARPES data.

II. METHODOLOGY

In the calculations, the Si(001) surface is modeled by setting up orthorhombic supercells with slabs each consisting of 12 monolayers of silicon, which are decoupled by a more than 25 Å thick vacuum layer in z direction. The lateral dimensions are two surface unit cells parallel to the nanowire growth direction ([110], y direction) due to the presence of the buckled dimers on the surrounding Si(001)-(2 × 2) surface, and 16 unit cells orthogonal to the wires ([1$\bar{1}$0], x direction) in order to consistently separate the nanowires. Hydrogen atoms saturate the dangling bonds at the lower side of the slabs and are kept fixed during relaxations together with the lowest four monolayers of silicon.

Erbium is employed as a prototypical RE, which can be considered representative for all trivalent RE. The trivalent RE only differ in their atomic radii (which slightly decrease with the atomic number) and in the number of $4f$ electrons, which increases with the atomic number. As the latter does not strongly influence the atomic structure (as we shall demon-

strate), and based on our experience with other RE silicide structures on Si(111) [21], the results obtained for erbium may be extended, at least qualitatively, to all trivalent RE.

We use the Vienna Ab initio Simulation Package to carry out all DFT calculations [22,23]. PAW potentials with the exchange-correlation energy treated within the GGA-PBE formalism are employed [24–26]. The plane wave cutoff is set to 450 eV and the Brillouin zone is sampled by a 2 × 16 × 1 Monkhorst-Pack mesh [27]. In order to calculate numerically converged total and site projected local density of states (DOS, LDOS), the k-point sampling has been increased to a 4 × 32 × 1 k-point mesh. Structural relaxation is stopped when all Hellman-Feynman forces are smaller than 5 meV/Å [29]. The $4f$ electrons of the RE are kept frozen in the core, as we have verified that they play a negligible role in the structural properties of stochiometric bulk hexagonal ErSi$_2$, leading only to variations in the lattice parameters smaller than 0.01 Å.

In order to determine the most favorable wire geometry, *ab initio* thermodynamics is used, with the Landau potential Ω as the central quantity [21,30,31].

$$\Omega(\mu_{\text{Si}}, \mu_{\text{Er}}) = \frac{1}{A}\left[F(N_{\text{Si}}, N_{\text{Er}}) - \sum_i^{\text{Si,Er}} \mu_i N_i\right]. \quad (1)$$

Following a common approach [30,32], the free energy F is approximated by the DFT total energy of the supercell E^{Cell} ($T = 0$ K) and the chemical potential of silicon μ_{Si} is set to the one in bulk silicon $\mu_{\text{Si}}^{\text{Bulk}}$ (silicon rich conditions). μ_{Er} is a free parameter, reflecting the growth conditions. As Er atoms are bound in a stoichiometric ErSi$_2$ crystal structure in nanowires, we vary μ_{Er} in range around $\mu_{\text{Er}}^{\text{ErSi}_2}$. The latter value differs by only few 10 meV between the hexagonal and tetragonal ErSi$_2$ bulk. μ_{Er} values larger than $\mu_{\text{Er}}^{\text{Bulk}} = -4.6$ eV would result in Er segregation on the Si(001) surface.

The supercell can be separated into two parts, one part representing the clean surface with area A_{C} and the other consisting of the nanowire with area A_{W} (see Fig. 2). A_{C} corresponds to an half-integral number of the Si(001)-(2 × 2) unit cell. As A_{C} might change with the burial depth for the same wire, the Landau potential of structures with the same number of Er atoms might have a different slope in with respect to μ_{Er}. As test calculations show that these two parts are energetically independent, we subtract $A_{\text{C}}\Omega^{\text{C}}$ from E^{Cell} to obtain E^{W}. With E^{W} and A_{W} we calculate the Landau potential of the nanowire and refer it to the one of the clean surface.

$$\Omega^{\text{W}}(\mu_{\text{Si}}, \mu_{\text{Er}}) = \frac{1}{A_{\text{W}}}\left(E^{\text{W}} - \sum_i^{\text{Si,Er}} \mu_i N_i^{\text{W}}\right) - \Omega^{\text{C}}. \quad (2)$$

A schematic overview of the nanowire models explored in this work is shown in Fig. 2. The figure shows two examples for optimized structures of 5a wide (a is the Si surface lattice constant) and two layers high nanowires consisting of the hexagonal silicide, (a) with the c axis perpendicular to the nanowire direction [denoted R (rectangular appearance in cross-sectional view)] and (b) with the c axis parallel [denoted H (hexagonal appearance)]. The selected width and height represent the typical parameters found experimentally [17]. The nanowires represented in the picture are buried by one
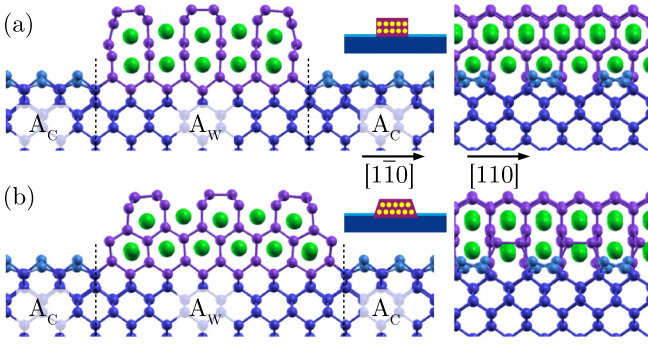
FIG. 2. Optimized structures of $5a$ wide and two layers high nanowires buried into the substrate by one layer (a) with the hexagonal c axis perpendicular (labeled R) and (b) parallel to the nanowire direction (labeled H), in cross-sectional view (left) and side view (right). Blue circles indicate Si substrate atoms, light blue circles the Si dimers of the clean Si(001) surface, magenta circles Si atoms in the nanowires, and green circles Er atoms. A_W and A_C indicate the areas of the nanowire and of the clean substrate, respectively. The schematic representation shown in the central part will be used in the following to indicate the discussed structures [28].

layer into the substrate. In their center, the structures nicely represent the bulk silicide structure, while some deviations at the sides such as dimer formation occur in particular in the case of the H structure. Many different types of wire sides (symmetric, asymmetric, plane, and corrugated) have been modeled. The most stable side configurations depend on the burial depth and are shown in the supplemental material [34].

Moreover, the nanowire tops are generally modeled with Si dimer chains along the nanowires leading to a (2×1) reconstruction, as observed in Fig. 1(b) as well as in other experi-

ments [3,17,19]. We have verified this assumption by modeling dimer-induced reconstructions of different periodicity. Independently on the wire structure, the (2×1) reconstruction is always energetically favored. For simplicity, the substrate surface besides the nanowires is modeled by a Si(001)-(2×2) surface with the thermally frozen asymmetric dimers and dimer chains oriented perpendicular to the nanowires [17], although in reality a RE containing wetting layer with an up-to-now undetermined structure is formed [14,17–19]. This is justified since the wetting layer is electronically decoupled from the nanowires. Moreover, the wetting layer has the same periodicity as the substrate, so that we do not expect it to differently influence nanowires of different width and height. Thus, the wetting layer will mainly lead to a constant offset in the absolute formation energy of the nanowires, without modifying their relative stability.

III. RESULTS

A multiplicity of models (about 70) has been tested in order to determine the most stable nanowire structures. For this purpose, four degrees of freedom are considered: the orientation of the hexagonal unit cell, the depth of burial into the substrate as well as the height and the width of the nanowires. Due to this systematic approach, the investigated geometries include all structural models previously proposed. Starting from the models shown in Fig. 2, the other degrees of freedom are varied, first independently and then simultaneously. The results are shown in Fig. 3.

At first the burial depth is varied, as shown in Figs. 3(a) and 3(d). Irrespective of the Er chemical potential, an optimum depth of two Si layers is found for both the R and the H structure. The calculations are then repeated for sample wires of different width and height, confirming that the burial depth
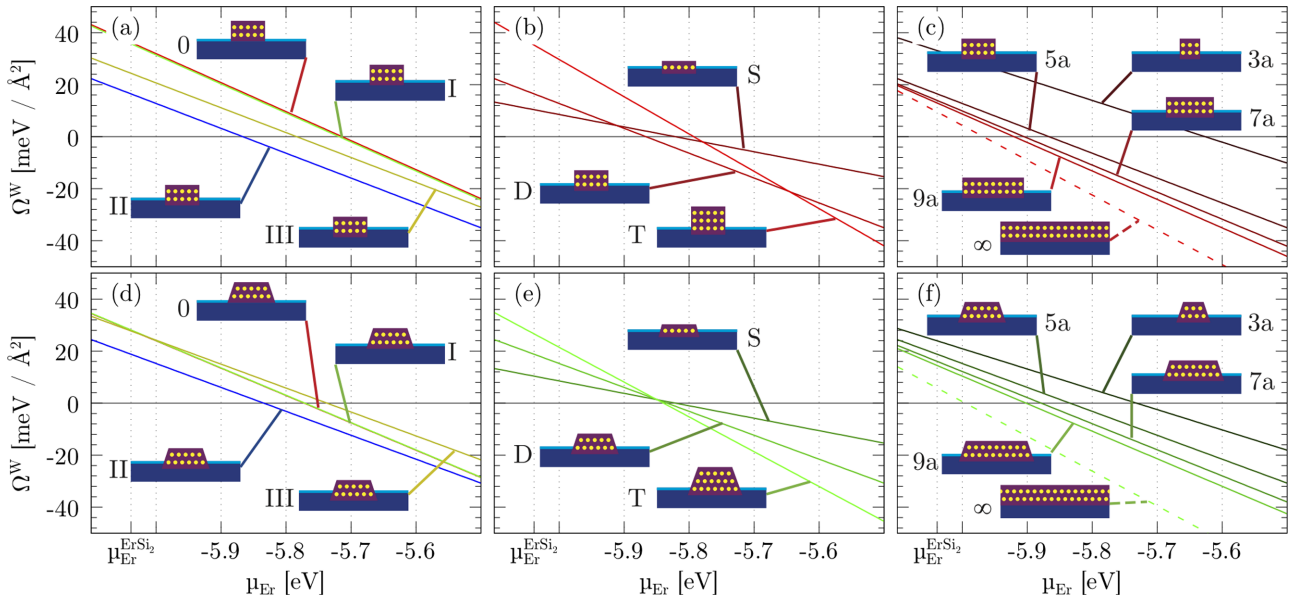
FIG. 3. Variation of the Landau potential [(a) and (d)] for different burial depths, [(b) and (e)] for different nanowire heights, and [(c) and (f)] for different nanowire widths, [(a)–(c)] for the R and [(d)–(f)] for the H structures. 0–III denote the depths varying from 0 to 3 silicon monolayers, S, D, and T stand for single, double, and triple height, respectively, and 3a–9a and ∞ indicate the widths of the nanowire in multiples of silicide unit cells.

of two Si layers leads to the lowest formation energies for given widths, heights, and silicide orientations.

Using this depth and the $5a$ broad wires, the height is systematically varied for the R and H structures, as shown in Figs. 3(b) and 3(e). For increasing μ_{Er} values, higher wires with a proportionally higher Er content are thermodynamically favored. While this trend is clearly visible for wires with the R structure [Fig. 3(b)], wires with the H structure and two silicide layers height are stable only in an extremely narrow μ_{Er} range [Fig. 3(e)]. Again, sample tests with wires of different burial depth confirm that the the optimal wire height depends on the Er availability.

Finally, using models that are two layers high and buried by two Si layers into the surface, the wire width is varied for the R and H structures [Figs. 3(c) and 3(f)]. Here, only odd numbers of unit cells were considered to account for the (2×1) nanowire surface structure. The Landau potential drops for larger widths, reaching its minimum, irrespective of the chemical potential of erbium, for infinitely broad wires. This represents the complete coverage of the silicon surface with ErSi$_2$ silicides, as observed in the case of the Si(111) structure [21]. For this coverage, the R and H structure are equivalent, except for a different orientation of the top silicon dimers. However, the energy differences between these two-dimensional ErSi$_2$ coverages are small, amounting only to values below 4 meV/Å^2. A similar trend ist also observed for heights of one or three atomic layers.

It should be noted that for $\mu_{Er} \approx \mu_{Er}^{ErSi_2}$ no wire model has a Landau potential below the one of the clean surface ($\Omega^C = 0$). This is quite surprising, as consequently, the simultaneous presence of a clean silicon surface and bulk ErSi$_2$ is thermodynamically stable, while the nanowires are metastable. Indeed, for high annealing temperatures RESi$_2$ islands and an otherwise clean Si(001) surface form instead of nanowires [17], which indicates that the nanowires are metastable.

As pure themodynamic stability cannot be addressed as the driving force for the wire formation, kinetic effects, such as an anisotropic surface diffusion [14,15], probably lead to the formation of the metastable nanowires. The anisotropic surface diffusion has been previously explained by the lattice mismatch between RE silicide and substrate [8]. While a homogeneously strained silicide layer represents the global minimum of the energy hypersurface, it can be hardly formed during growth. Stacking faults and dislocations, not included in our models, might be expected for the 2D silicide layers. Moreover, the formation of nanowire bundles [see Fig. 1(a)], which could not be analyzed here due to the system size, may further modify the energy of the nanowires.

When comparing the Landau potential of the R and H structures for the experimentally most frequent $5a$ wide and two layers high nanowires, the differences are smaller than 3 meV/Å^2 for $\mu_{Er} \approx \mu_{Er}^{ErSi_2}$, being equal to 50 meV per unit cell. This value is below the thermal energy under preparation conditions ($k_B T > 70$ meV) and indicates that wires with both orientations of the RESi$_2$ have substantially the same formation energy. This result seems surprising when considering the lattice mismatch of about 7% in c direction already mentioned above, which should strongly favor the less strained R structure. However, the reported lattice constants of
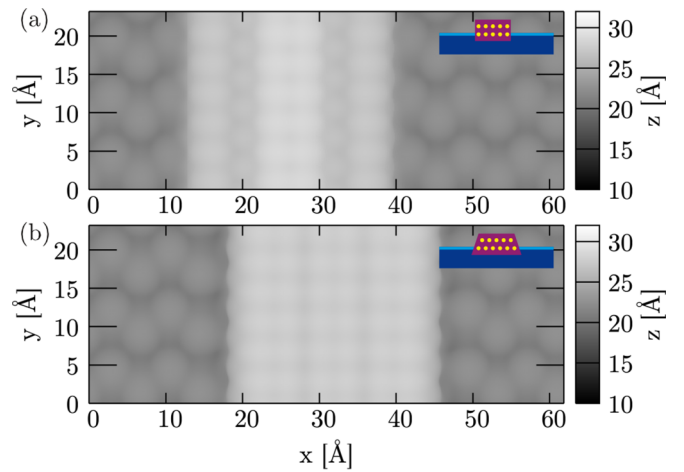
FIG. 4. Simulated STM-images (sample voltage $V_{sample} = -1.5$ V, filled states) for slabs modeling the ErSi$_2$ nanowires (a) with R structure and (b) with H structure according to the thermodynamically stable models of $5a$ width.

the RESi$_2$ bulk crystals were experimentally determined for silicides with a considerable concentration of silicon vacancies, resulting in an actual RESi$_{2-x}$ stoichiometry with $x \approx 0.3$ [33]. Yet, no indications for such vacancies were observed experimentally for the nanowires. While our calculations of nonstoichiometric ErSi$_{1.7}$ bulk crystals roughly reproduce the experimental c/a ratio of about 1.08, calculations of vacancy-free ErSi$_2$ bulk crystals yielded a c/a value of 0.95, so that the anisotropic lattice mismatch cannot be considered as an argument for the formation of nanowires with R orientation. The situation is similar for the other trivalent RE [33]. Indeed, recent atomically resolved TEM data clearly show that terbium silicide nanowires are characterized by the H Structure [11].

After analyzing the thermodynamical stability of different nanowire models, we check whether they are compatible with available STM and ARPES data. Therefore we simulate STM images and derive the band structures for nanowire models partially buried into the substrate and two silicide monolayers high [34] and compare the results with the experimental data.

Simulated constant-current STM images are calculated within the Tersoff-Hamann model [35,36] for the nanowires of $5a$ width with R and H orientation. In the simulated STM images (filled states, Fig. 4) the nanowires appear as rather homogeneous bright rows along the nanowires with darker ridges in between. The latter separate the dimer rows on top of the nanowires. Thus, the $5a$ broad wires, on top of which three dimer rows are formed, appear as triple row of almost identical dimer chains. This is in very good agreement with the experimental STM images [see Fig. 1(b)]. As in the corresponding STM experiments, the simulated empty states STM-images are qualitatively similar to the filled states STM images and are thus not shown here. As mainly the dimer rows are mapped in the STM images, which are present in similar form in all nanowires models, the simulated STM images achieved with different orientations show no appreciable difference. Consequently, the mere analysis of the STM
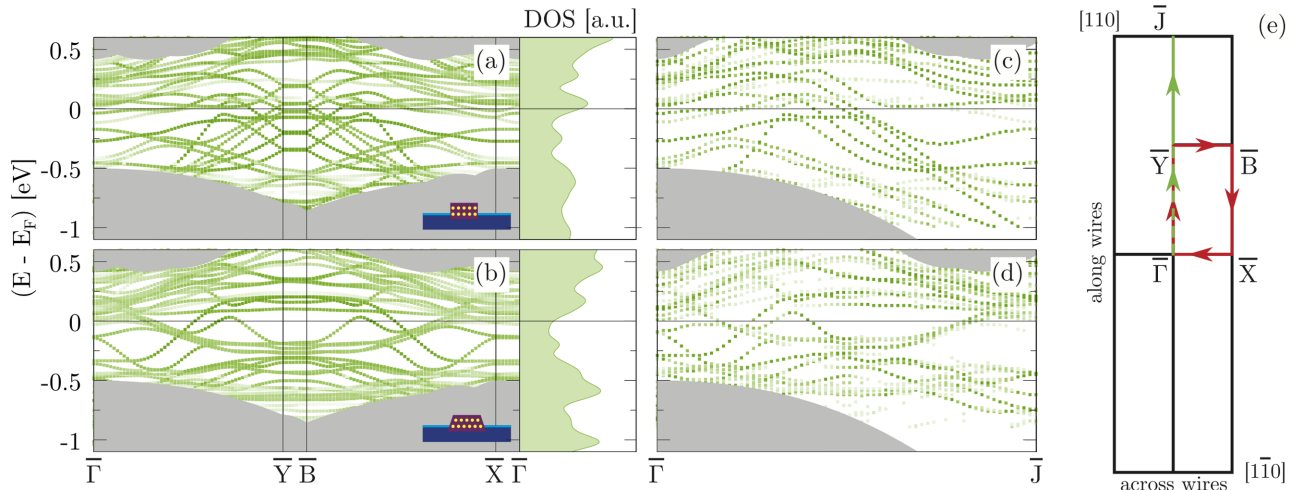
FIG. 5. [(a) and (b)] Band structure (left-hand side) and DOS (right-hand side) for the (a) R and (b) H structures of $5a$ broad nanowires with double height and buried into the substrate by two silicon layers. The intensity of the color in the band structure is proportional to the Er contribution. The gray overlay is the silicon bulk band structure projected onto the surface Brillouin zone. The panels on the right-hand side of (a) and (b) show the density of states (DOS/a.u.) integrated over the whole Brillouin zone and projected onto the Er atoms. The corresponding unfolded band structures are shown in (c) and (d). Panel (e) shows a sketch of the surface Brillouin zone with the relevant high symmetry points. All energies are given with respect to the slab Fermi energy E_F.

images is not sufficient to differentiate between structural models.

Finally, the electronic structure of the finite $5a$ broad R and H structures is calculated and compared to ARPES measurements. The theoretical results are shown in Figs. 5(a) and 5(b). In order to highlight the contributions of the nanowires and supressing those of the neighboring silicon surface, the electronic densities are weighted by projections of the wave functions onto spherical harmonics centered around atoms within a specific atom group and renormalized by the number of considered atoms. This represents the contribution of the atom group to the electronic band structure.

Both R and H structures exhibit bands that are strongly dispersive parallel to the nanowires ($\bar{\Gamma}$-$\bar{Y}$ direction) and strongly localized perpendicular to it ($\bar{\Gamma}$-$\bar{X}$ direction). There is no band gap, so that the nanowires form a one-dimensional metallic system. For each structural model, a multitude of states exists within the band gap of the silicon substrate due to the large number of atoms in the unit cell, which renders the band structures very complex. The main contribution is given by the nanowire states (erbium + silicon cage). The band structures of the erbium atoms and the nanowire cage look qualitatively alike, while quantitatively the erbium atoms contribute much more to the DOS than the cage. A closer analysis shows that the nanowire states are completely decoupled from the substrate and its surface dimer states. The latter, which are dispersive for the clean (2×2) reconstructed Si(001) surface, are well localized, in accordance with the interruption of the dimer chains by the nanowire leading to the creation of quantum wells.

While the supercell has a $2a$ periodicity in nanowire growth direction because of the surrounding Si surface, the nanowires themselves are characterized by a $1a$ periodicity [with the exception of a dimerization at the side flanks of the H structure that may be neglected, see Fig. 2(b)]. In order to compare the

theoretical results with the ARPES measurements, where no indications of the $2a$ periodicity were found [9], the calculated band structure was unfolded using the BandUP code [37,38]. The results are shown in Figs. 5(c) and 5(d), with the extended surface Brillouin zone displayed in Fig. 5(e).

In Fig. 6, the experimentally derived bands from Fig. 1(c) are overlaid by the unfolded band structure from Figs. 5(c) and 5(d). A good matching is obtained when the calculated bands are shifted to lower energies by about 0.2 eV, since the experimentally observed Fermi energy lies about 0.2 eV below the conduction band minimum [9]. This deviation can be explained by a charge transfer from the experimentally observed RE silicide wetting layer, which is actually present besides the nanowires instead of the clean Si(001)-(2×2) surface assumed in the present calculations.

We remark that in order to present a consistent set of data calculated for ErSi$_2$ (including structures, energetics, calculated STM images, and band structures) we use the calculated ErSi$_2$ nanowire band structure for the comparison with the experimental STM and ARPES data from TbSi$_2$ nanowires. This is justified by the fact that the band structures calculated for ErSi$_2$ and TbSi$_2$ nanowires are practically indistinguishable [39].

Because of the complexity of the theoretical band structures, a conclusive assignment of the ARPES bands to the R or H structure is not possible on the basis of the comparison shown in Fig. 6. Both structures are roughly compatible with the ARPES data, although the dispersive bands around $\bar{J}$ seem to be better reproduced by the H structure. However, a direct comparison of experimental ARPES data with calculated band structures is difficult. While all electronic states appear in the theoretical models, not all electronic states are visible at the same time in ARPES records. This is due to matrix element effects, which are known to strongly influence the ARPES data of rare-earth silicide nanowires on Si(001) [9].

a certain smearing of the recorded states. Taking in account these sources of uncertainty, and the intrinsic error of DFT calculations, the agreement between measured and calculated data can be considered satisfactory.

IV. CONCLUSION

In summary, we investigated erbium silicide nanowires on the Si(001) surface by density functional theory and compared theoretical results to experimental findings. The nanowires are found to be metastable, as their width is not limited by thermodynamics, so that an infinite coverage of the substrate with a two-dimensional erbium silicide film represents the thermodynamical ground state. Thus the experimental observation of the silicide nanowires suggests that kinetic effects play a dominant role. The nanowires of finite width were categorized corresponding to four degrees of freedom. Nanowire models that are buried into the silicon surface by two silicon layers turned out to be energetically favored with respect to wires with different bural depths. The height of the nanowires depends on the chemical potential of erbium, favoring higher models for larger deposition amounts. Turning the nanowire supercell by 90° (i.e., switching from the R to the H structure) leads to small energy differences that are below the thermal energy under experimental conditions. Both the R and H structure exhibit a similar surface structure and one-dimensional metallicity, in agreement with experimental STM and ARPES data.

FIG. 6. Electronic states of the (a) 5*a*-R and (b) 5*a*-H structures [calculated for nanowires of double height and buried into the substrate by two silicon layers] overlaid to the measured ARPES data. See text for details.

Furthermore, ARPES seems to be characterized by larger cross sections for highly dispersive states than for strongly localized states, which then usually appear with a reduced relative intensity [40]. Moreover, the signal from the nanowires is superposed by the one from the surrounding and usually rather disordered wetting layer, resulting in a lower signal-to-noise ratio. Finally, the experimental data display the averaged band structure of wires of different widths, which results in

[1] Y. Chen, D. A. A. Ohlberg, G. Medeiros-Ribeiro, Y. A. Chang, and R. S. Williams, Appl. Phys. Lett. **76**, 4004 (2000).

[2] J. Nogami, B. Z. Liu, M. V. Katkov, C. Ohbuchi, and N. O. Birge, Phys. Rev. B **63**, 233305 (2001).

[3] C. Preinesberger, S. K. Becker, S. Vandré, T. Kalka, and M. Dähne, J. Appl. Phys. **91**, 1695 (2002).

[4] Z. He, D. J. Smith, and P. A. Bennett, Phys. Rev. B **70**, 241402(R) (2004).

[5] Y. Cui and J. Nogami, Surf. Sci. **605**, 2038 (2011).

[6] C. Preinesberger, G. Pruskil, S. K. Becker, M. Dähne, D. V. Vyalikh, S. L. Molodtsov, C. Laubschat, and F. Schiller, Appl. Phys. Lett. **87**, 083107 (2005).

[7] H. W. Yeom, Y. K. Kim, E. Y. Lee, K. D. Ryang, and P. G. Kang, Phys. Rev. Lett. **95**, 205504 (2005).

[8] M. Wanke, K. Löser, G. Pruskil, D. V. Vyalikh, S. L. Molodtsov, S. Danzenbächer, C. Laubschat, and M. Dähne, Phys. Rev. B **83**, 205417 (2011).

[9] S. Appelfeller, M. Franz, H.-F. Jirschik, J. Große, and M. Dähne, New J. Phys. **18**, 113005 (2016).

[10] I. Miccoli, F. Edler, H. Pfnür, S. Appelfeller, M. Dähne, K. Holtgrewe, S. Sanna, W. G. Schmidt, and C. Tegenkamp, Phys. Rev. B **93**, 125412 (2016).

[11] S. Appelfeller, J. Heggemann, T. Niermann, M. Lehmann, and M. Dähne, Appl. Phys. Lett. **114**, 093104 (2019).

[12] S. Appelfeller, M. Franz, M. Kubicki, P. Reiß, T. Niermann, M. A. Schubert, M. Lehmann, and M. Dähne, Appl. Phys. Lett. **108**, 013109 (2016).

[13] Y. Chen, D. A. A. Ohlberg, G. Medeiros-Ribeiro, Y. A. Chang, and R. S. Williams, Appl. Phys. A **75**, 353 (2002).

[14] C. Eames, M. Reakes, S. P. Tear, T. C. Q. Noakes, and P. Bailey, Phys. Rev. B **82**, 174112 (2010).

[15] C. Eames, M. I. J. Probert, and S. P. Tear, Appl. Phys. Lett. **96**, 241903 (2010)

[16] M. Dähne and M. Wanke, J. Phys.: Condens. Matter **25**, 014012 (2013).

[17] S. Appelfeller, S. Kuls, and M. Dähne, Surf. Sci. **641**, 180 (2015).

[18] V. Iancu, P. R. C. Kent, S. Hus, H. Hu, C. G. Zeng, and H. H. Weitering, J. Phys.: Condens. Matter **25**, 014011 (2013).

[19] V. Iancu, P. R. C. Kent, C. G. Zeng, and H. H. Weitering, Appl. Phys. Lett. **95**, 123107 (2009).

[20] N. Gonzalez Szwacki and B. I. Yakobson, Phys. Rev. B **75**, 035406 (2007).

[21] S. Sanna, C. Dues, W. G. Schmidt, F. Timmer, J. Wollschläger, M. Franz, S. Appelfeller, and M. Dähne, Phys. Rev. B **93**, 195407 (2016).

[22] G. Kresse and J. Furthmüller, J. Comput. Mater. Sci. **6**, 15 (1996).

[23] G. Kresse and J. Furthmüller, Phys. Rev. B **54**, 11169 (1996).

[24] P. E. Blöchl, Phys. Rev. B **50**, 17953 (1994).

[25] G. Kresse and D. Joubert, Phys. Rev. B **59**, 1758 (1999).

[26] J. P. Perdew, K. Burke, and M. Ernzerhof, Phys. Rev. Lett. **77**, 3865 (1996).

[27] H. J. Monkhorst and J. D. Pack, Phys. Rev. B **13**, 5188 (1976).

[28] A. Kokalj, Comput. Mater. Sci. **28**, 155 (2003).

[29] R. P. Feynman, Phys. Rev. **56**, 340 (1939).

[30] S. Sanna and W. G. Schmidt, Phys. Rev. B **81**, 214116 (2010).

[31] F. Bechstedt, *Principle of Surface Physics* (Springer, Berlin, 2003).

[32] S. Sanna, C. Thierfelder, S. Wippermann, T. P. Sinha, and W. G. Schmidt, Phys. Rev. B **83**, 054112 (2011).

[33] J. A. Knapp and S. T. Picraux, Appl. Phys. Lett. **48**, 466 (1986).

[34] See Supplemental Material at http://link.aps.org/supplemental/10.1103/PhysRevB.99.214104 for S1.pdf containing cross-sectional images of 5a-D-II-R and 5a-D-II-H structure. The corresponding Crystallographic Information Files [CIF] are also available [5a-D-II-R.cif and 5a-D-II-H.cif].

[35] J. Tersoff and D. R. Hamann, Phys. Rev. Lett. **50**, 1998 (1983).

[36] J. Tersoff and D. R. Hamann, Phys. Rev. B **31**, 805 (1985).

[37] P. V. C. Medeiros, S. S. Tsirkin, S. Stafström, and J. Björk, Phys. Rev. B **91**, 041116(R) (2015).

[38] P. V. C. Medeiros, S. Stafström, and J. Björk, Phys. Rev. B **89**, 041407(R) (2014).

[39] See Supplemental Material at http://link.aps.org/supplemental/10.1103/PhysRevB.99.214104 for S2.png containing a comparison of unfolded band structures of Er and Tb wires [5a-D-II-R structure].

[40] S. Sanna, T. Lichtenstein, Z. Mamiyev, C. Tegenkamp, and H. Pfnür, J. Phys. Chem. C **122**, 25580 (2018).